ACTA ASTRONOMICA
Vol. **46** (1996) pp. 0–0

CPPA – a New Hydrodynamical Code for Cosmological Large-Scale Structure Simulations

by

Andrzej Kudlicki[1] Tomasz Plewa[2] Michał Różyczka[3,1]

[1] Nicolaus Copernicus Astronomical Center, Bartycka 18, 00-716 Warszawa, Poland
e-mail:kudlicki@camk.edu.pl
[2] Max-Planck-Institut für Astrophysik, Karl-Schwarzschild-Str. 1, 85740 Garching, Germany
e-mail:tomek@MPA-Garching.MPG.DE
[3] Warsaw University Observatory, Al. Ujazdowskie 4, 00-478 Warszawa, Poland
e-mail:mnr@camk.edu.pl

Received August 14, 1996

ABSTRACT

We present a new Eulerian code able to follow the evolution of large-scale structures in the Universe in the weakly nonlinear regime. We compare test results with a N-body code and analytical results.

Key words: *cosmology: large-scale structure of Universe – methods: numerical*

1. Introduction

The Universe is homogeneous on scales larger than at least 100 Mpc. Therefore, any simulations intended to completely predict the development of structures ought to work with a dynamical range 10 kpc–100 Mpc. A disadvantage of this fact is that enormous catalogues of galaxies are needed for a comparison of models of large-scale structure versus observations. The first sufficient catalogue will be the SDSS (Gunn and Knapp 1993), to come within a few years. On the other hand, a great advantage of examining very large scale structures is that density contrasts on these scales are relatively low (*i.e.*, weakly nonlinear, with $\delta = \frac{\rho - \overline{\rho}}{\overline{\rho}} < 1$), and various fields observed (convolved) with large windows can be worked on either with the use of analytical methods (like perturbation theory) or numerical simulations with simplified physics (*e.g.*, effects of pressure, radiation *etc* can be neglected). Even in the weakly nonlinear regime there are many features which have not been examined with analytical methods, *e.g.*, moments of projected velocities or redshift

distortions. All of the above give a good reason for writing a new, fast code, able to follow the evolution of structure in various cosmological models.

We present a new Eulerian code, which can be applied to linear and weakly non-linear evolutionary stages of dense regions of the Universe and to trace the voids (N-body codes are not good for describing low density regions). The code is tested and the results are compared with theoretical predictions, as well as with results obtained from modified $\mathrm{AP^3M}$ N-body code by Couchman (1991),(1994).

2. Numerical Method

2.1. Description

Cosmological Pressureless Parabolic Advection (CPPA) is an Eulerian code, solving the dynamical equations of a self-gravitating pressureless fluid (Poisson, continuity and Euler).

$$\frac{\partial^2 \Phi}{\partial r^i \partial r^i} = 4\pi G \varrho \tag{1}$$

$$\frac{\partial \varrho}{\partial \tau} + \frac{\partial \varrho u^k}{\partial r^k} = 0 \tag{2}$$

$$\frac{\partial \varrho u^i}{\partial \tau} + \frac{\partial \varrho u^i u^k}{\partial r^k} + \varrho \frac{\partial \Phi}{\partial r^i} = 0 \tag{3}$$

The code works with a fixed and uniform 3-D Cartesian grid in cosmological frame. Periodic boundary conditions are employed, which do not introduce any systematic deviations at grid boundaries, and are easy to implement for solving Poisson equation using Fourier methods. The Poisson solver is adapted from a standard Helmholtz equation solving routine available in *FISHPAK* library (Adams, Schwarztrauber, and Sweet 1980).

The advection algorithm is based on the PPM method of Colella and Woodward (1984) with pressure terms set to zero. We replaced the nonlinear Riemann solver by a simple procedure which defines the interface values as the upwind value equal to one of the effective states averaged over domains of dependence in neighboring zones. Since there is no sufficient justification for steepening of the density jumps we did not use PPM steepening algorithm. Also, the whole set of dissipation procedures is not needed for present application. The temporal evolution is accurate to second order while the spatial advection is formally third order accurate. The non-cosmological version of the code has been widely tested and proved isotropic and precisely solving Euler and Poisson equations.

To adapt the code for cosmological purposes we changed the variables and coordinates in Eq. (1)–(3) following the recipe given by Gnedin (1995). Let τ, r^i, u^i, ϱ, Φ denote time, positions, velocities, density and gravitational potential in physical units. We define new set of variables t, x^i, v^i, ρ and ϕ given by Eqs (4)–(8):

$$\mathrm{d}\tau = \frac{a^2}{\mathrm{H}_0}\mathrm{d}t, \tag{4}$$

$$r^i = aLx^i, \tag{5}$$

$$u^i = \frac{da}{dt}Lx^i + \frac{L\mathrm{H}_0}{a}v^i, \tag{6}$$

$$\varrho = \frac{3\mathrm{H}_0^2\Omega_0}{8\pi G a^3}\rho, \tag{7}$$

$$\Phi = \left(\frac{L\mathrm{H}_0}{a}\right)^2 \phi - \frac{aL^2x^ix^i}{2}\frac{d^2a}{d\tau^2}, \tag{8}$$

where a is the scale factor, H_0 is the Hubble constant today, Ω_0 is the dimensionless density parameter today, G denotes the gravitational constant and L is a dimensional parameter denoting the computational box size. The density ρ has been scaled to $\langle\rho\rangle = 1$, so $\rho = 1 + \delta$. In these coordinates, assuming that scale factor changes with time according to Friedmann-Robertson-Walker solution, equations Eq. (1)–(3) are

$$\frac{\partial^2\phi}{\partial x^i \partial x^i} = \frac{3a\Omega_0}{2}\delta, \tag{9}$$

$$\frac{\partial\rho}{\partial t} + \frac{\partial(\rho v^k)}{\partial x^k} = 0, \tag{10}$$

and

$$\frac{\partial(\rho v^i)}{\partial t} + \frac{\partial(\rho v^i v^k)}{\partial x^k} + \rho\frac{\partial\phi}{\partial x^i} = 0. \tag{11}$$

The form of Eqs (9)–(11) is very similar to Eqs (1)–(3), expressed in physical coordinates, which makes it relatively easy to adapt any hydrodynamical code to work in the cosmological frame. For a given cosmological model, only the functions $a(t)$ and $\tau(t)$ have to be evaluated numerically before the simulation is started. The present version works with $\Lambda = 0$, but it can be easily modified to deal with models with a non-zero cosmological constant, which requires only adding one more term to Eq. (9).

2.2. Initial Conditions

For cosmological simulations we assume a Gaussian distribution of the initial density contrast, δ, with a given power spectrum and amplitude in the linear regime ($\langle\delta^2\rangle^{\frac{1}{2}} \leq 0.05$). First, the initial density field $\delta(\vec{x})$ is set up in the form of its Fourier transform $\tilde{\delta}(\vec{k})$, with amplitudes according to a given power spectrum and phases chosen randomly. To keep the density field real we impose

$$\tilde{\delta}(-\vec{k}) = \tilde{\delta}(\vec{k})^\star. \tag{12}$$

To prevent exceeding the Nyquist frequency, the spectra are multiplied by $e^{-(k/k_{\mathrm{cut}})^{16}}$, where k_{cut} is smaller than k_{Nq} (typically, we used $k_{\mathrm{cut}}/k_{Nq} = 0.5 \ldots 0.7$). Next,

the field is Fourier-transformed back to the real space. Simulations of cosmological large-scale structure are started at early stages, when the linear approximation in the perturbation theory (see *e.g.*, Peebles 1980, §11) can be applied. According to this approximation

$$\delta = A_1 D_1(\tau) + A_2 D_2(\tau), \tag{13}$$

where D_1 and D_2 denote the growing and decaying modes respectively. We assume that our starting evolutionary stage is advanced enough for not taking the decaying mode into account, *i.e.*, $D_2(\tau_{\rm start}) \ll D_1(\tau_{\rm start})$. From the continuity Eq. (2) we find that the initial velocity $\vec{u}$ and density contrast δ are then related as follows:

$$\frac{{\rm d}\delta}{{\rm d}\tau} + \frac{1}{a}\nabla \cdot \vec{u} = 0. \tag{14}$$

Hence,

$$\nabla \cdot \vec{u} = -a{\rm H}f\delta, \tag{15}$$

where H is the current value of the Hubble's expansion parameter and f is given by

$$f = \frac{a}{D_1}\frac{{\rm d}D_1}{{\rm d}a} = \frac{a}{D_1}\frac{{\rm d}D_1}{{\rm d}\tau}\frac{1}{{\rm d}a/{\rm d}\tau} = \frac{1}{\rm H}\frac{\dot{D}_1}{D_1}$$

and can be well approximated by

$$f \approx \Omega^{0.6} + \frac{\Omega_\Lambda}{70}\left(1 + \frac{1}{2}\Omega\right).$$

Ω denotes here the density parameter at $\tau_{\rm start}$, and $\Omega_\Lambda = \Lambda/3{\rm H}^2$ is related to the cosmological constant. The vector field $\vec{u}$ is then the gradient of a scalar field ψ, defined by the Poisson equation

$$\triangle\psi = a{\rm H}f\delta. \tag{16}$$

Therefore, given the density, the Poisson solver can be used for evaluating the initial velocity field.

3. The AP^{3}M Code

Our comparison code is the adaptive P^{3}M developed by Couchman (1991),(1994). In this paper we will note only our changes to the code. Apart of altering the program's I/O we made two major changes. First of them was to introduce a CFL type evaluation of next time-step length. The second one was to change the time coordinate as explained below, and adapt the code to work in cosmological frame with $\Omega \neq 1$, which was not supported by the original version. In comoving coordinates, the equation of motion of i-th particle in the expanding Universe reads

$$\frac{{\rm d}^2\vec{x}_i}{{\rm d}\tau^2} + 2\frac{\dot{a}}{a}\frac{{\rm d}\vec{x}_i}{{\rm d}\tau} = -\frac{G}{a^3}\sum_{j\neq i} m_j \frac{\vec{x}_i - \vec{x}_j}{|\vec{x}_i - \vec{x}_j|^3}, \tag{17}$$

where τ denotes the physical time and a the scale factor. As in CPPA, we will use another time variable, t, defined by Eq. (4). Eq. (17) will transform to:

$$\frac{\mathrm{d}^2\vec{x}_i}{\mathrm{d}t^2} = -a\frac{3\Omega_0 L^3}{8\pi N}\sum_{j\neq i}\frac{\vec{x}_i - \vec{x}_j}{|\vec{x}_i - \vec{x}_j|^3}, \tag{18}$$

where L is the computational box size and all of the N particles have mass equal $\frac{3\mathrm{H}_0^2\Omega_0 L^3}{8\pi G N}$, which is taken to be the mass unit. It is worth mentioning that by introducing t instead of physical time τ we have got rid of the cosmological drag term (in the original Couchman's version of the code time-stepping was performed at constant-length steps in a^α, where α is an arbitrary real exponent, and the calculations were time-staggered due to presence of the drag term).

4. Code Tests

The CPPA code has been tested versus the modified AP^{3}M and analytical results (the latter including both exact solutions and approximate calculations of the perturbation theory).

4.1. Zel'dovich Pancake Test

Zel'dovich Pancake is the final stage of the evolution of a single-wave perturbation, resulting in formation of a caustic. It may be also regarded as an idealization of a wall between two voids. The chief advantage of the pancake problem is that for $\Omega_0 = 1$ there exists an exact analytical solution:

$$\varrho(x,a) = R\left(1 - \frac{a}{a_c}\cos(kx)\right)^{-1},$$

where a_c is a parameter (the value of a at which an infinitely dense caustic is formed), and $R = \frac{\sqrt{a_c^2 - a^2}}{a_c}$ is the normalization factor. We performed this test on a 64^3 grid, setting up 1, 2, 4, 8 and 16 waves with initial dispersion 0.003 at an epoch corresponding to the scale factor equal to 0.001 of its present value. 1-D sections of the initial conditions are presented in Fig. 1. Fig. 2 shows the resulting pancakes at $a = 0.1$.

The density distribution in the AP^{3}M code is represented by the particle coordinates, actually it is a sum of N Dirac delta functions centered on each of the mass tracers. To obtain the grid-based density field, we convolved it with a Triangular Shaped Cloud (TSC) kernel function

$$U(x,y,z) = u(x)u(y)u(z),$$

where $u(x) = \frac{3}{4} - x^2$ for $|x| \leq \frac{1}{2}$, $u(x) = \frac{1}{2}(\frac{3}{2} - |x|)^2$ for $\frac{1}{2} \leq |x| \leq \frac{3}{2}$, and 0 elsewhere (the same kernel is used in the original AP^{3}M).

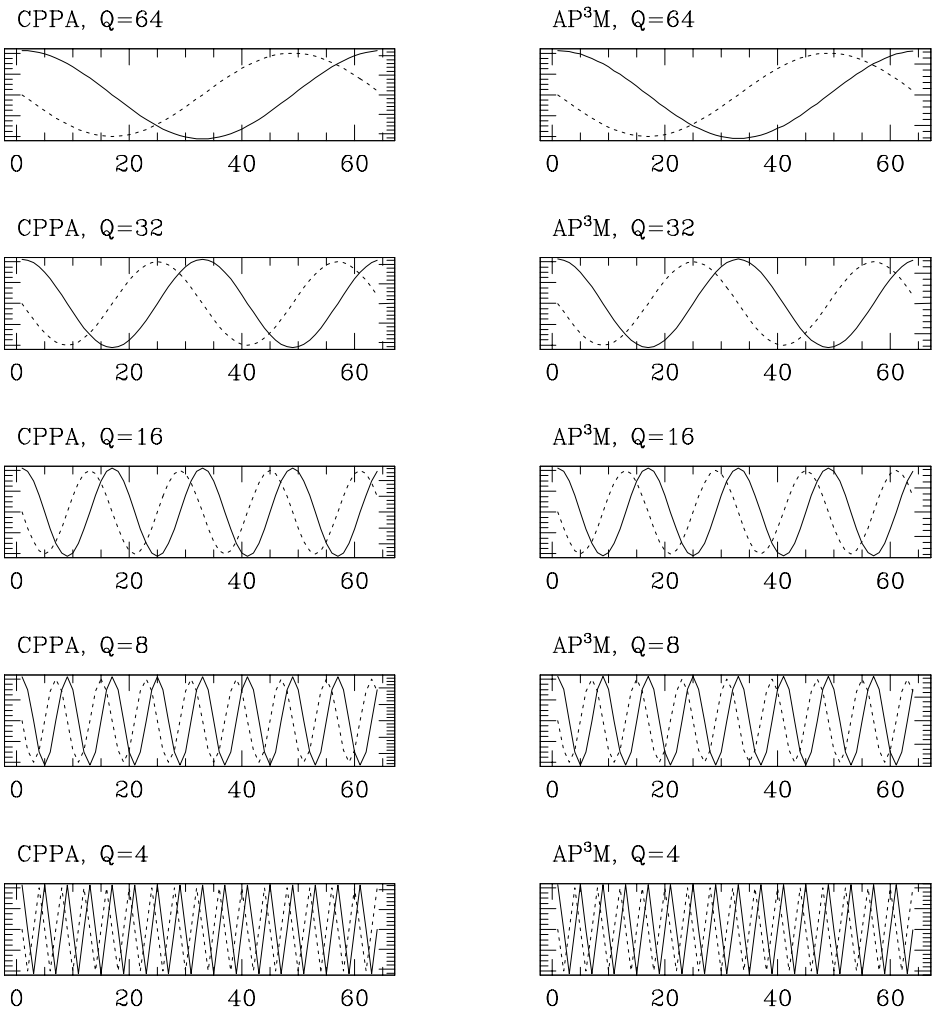

Fig. 1. 1-D sections through initial conditions for Zel'dovich pancake test on 64^3 grid.
Wavelength downwards: 64, 32, 16, 8 and 4 grid cells. **Left:** CPPA, **right:** AP^{3}M. **Solid line:** density profile (arbitrary scale) **dashed:** velocity profile (arbitrary scale).

A good quantitative measure of the departure of the obtained density field from the predicted theoretical value is the deviation of its variance. Integrating ϱ^2 over x one can obtain the density dispersion given by

$$\langle \delta^2 \rangle^{\frac{1}{2}} = \sqrt{\frac{a_c}{\sqrt{a_c^2 - a^2}} - 1}. \tag{19}$$

We obtain our results from a rectangular grid with cell size comparable to the regarded wavelengths (formally we are using a cubic top-hat filter). However, the predicted analytical value of $\langle \delta^2 \rangle^{\frac{1}{2}}$, given by Eq. (19), ought to be corrected for

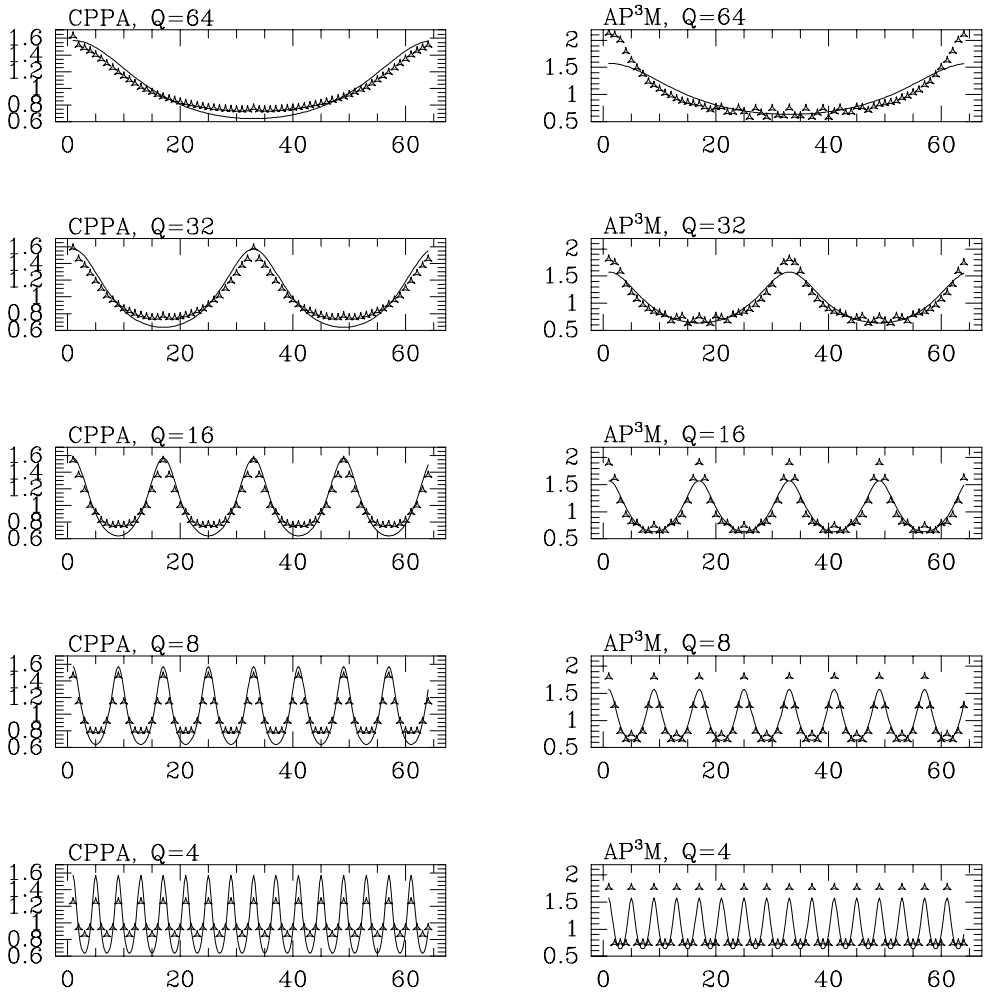

Fig. 2. 1-D sections through density profiles for Zel'dovich pancake test on 64^3 grid.
Horizontal axis: position, **vertical axis:** $\varrho/\langle\varrho\rangle$. Wavelength downwards: 64, 32, 16, 8 and 4 grid cells. **Left:** CPPA, **right:** AP^{3}M. **Solid line:** analytical results, **points:** simulation.

the effects of finite grid-cell size. Suppose our initial perturbation wavelength is Q times larger than a grid cell. The value of the predicted density dispersion on the grid is then given by

$$\langle\delta^2\rangle^{\frac{1}{2}}\Big|_Q = \sqrt{\frac{1}{Q}\sum_{p=0}^{Q-1}\left[\frac{Q}{2\pi}\int_{\frac{p}{Q}}^{\frac{p+1}{Q}}\varrho(x,a)\mathrm{d}x\right]^2 - 1}. \qquad (20)$$

In the weakly nonlinear regime the difference between Eq. (19) and Eq. (20) is small for long wavelengths, but it becomes important for waves with length of several grid cells (see Fig. 3f).

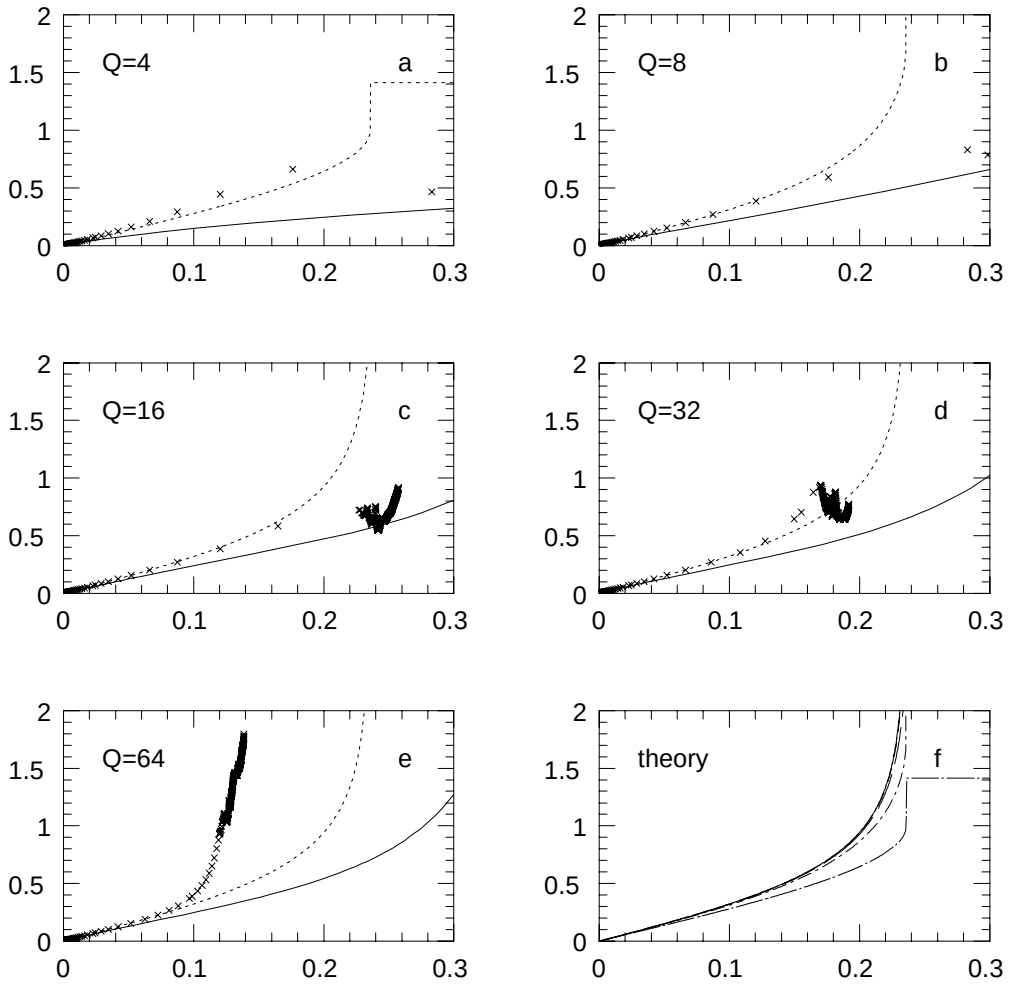

Fig. 3. Evolution of density dispersion in the Zel'dovich pancake test on 64^3 grid.
Horizontal axis: scale factor a, **vertical axis:** $\langle\delta^2\rangle^{1/2}$ **a–e**: simulation results for wavelengths of 4, 8, 16, 32 and 64 grid cells. **Solid line:** CPPA, **crosses:** AP^{3}M, **dashed line:** theoretical prediction. **f**: comparison of theoretical values given by Eq. (19) (**solid line**) to Eq. (20) for $Q = 64$ $Q = 32$ (**short dash**), $Q = 16$ (**long dash**), $Q = 8$ (**dot – short dash**), and $Q = 4$ (**dot – long dash**).

Results of this test for different wavelengths are plotted in Figs 3a–3e. As one can see, the evolution of a single wave is qualitatively correct in CPPA, but (especially for shorter waves) somewhat slower than predicted. The main reason for this is that at the final stage most of the mass is contained within walls one cell thick, *i.e.*, it has reached the resolution limit. The density dispersion curves generated with Couchman's code follow the theoretical curve closely until the particles come very close one to another. Then the accelerations become very high, the time step gets very short and oscillations of the wall due to interpenetration of particle streams

may start.

Upon comparing we can state that the CPPA code produces reasonably accurate solutions on scales larger than 4 grid cells.

4.2. Scale-free Models

Three simulations have been performed with each code. In CPPA we used a 128^3 grid, while in AP^{3}M 128^3 particles on a 128^3 grid. The models were started in an $\Omega = 1$ universe from Gaussian initial conditions with scale-free spectra (power indices +1, -1 and -3), cut-off below the Nyquist frequency, as explained in Section 2.2. For data reduction the density fields were convolved with a Gaussian window of FWHM = 8 cells.

The evolution of power spectra is shown in Fig. 4. CPPA as well as AP^{3}M conserve the power index on scales larger than 4 grid cells even in the nonlinear regime. The evolution of the density field cumulants $S_3 = \frac{\langle\delta^3\rangle}{\langle\delta^2\rangle^2}$ and $S_4 = \frac{\langle\delta^4\rangle - 3\langle\delta^2\rangle^2}{\langle\delta^2\rangle^3}$, compared to exact results obtained with the help of perturbation theory (Juszkiewicz, Bouchet, and Colombi 1993, Łokas *et al.* 1995) is presented in Fig. 5. Results from both codes are in reasonable agreement with each other and with theoretical predictions. The largest difference is for S_4 for $n = +1$, however this case often causes discrepancies (*e.g.*, Catelan and Moscardini (1994) in their Monte-Carlo computations obtained a value of 9 ± 1, while the perturbation theory gives $S_4 = 15.9$). Generally the agreement is better for models with lower power index, since in this case there is less power in small scales, on which the codes are less accurate.

Advanced evolutionary stages of the above CPPA and AP^{3}M models are shown in Fig. 6 in the form of 2-D slices through the density field. Additionally, we performed test runs with identical initial conditions for both CPPA and AP^{3}M. The tests were made on a 64^3 grid with CPPA and with 64^3 particles on a 64^3 grid in AP^{3}M. The initial spectral indices were -3 and $+1$. The runs were started at $z = 100$, with $\langle\delta^2\rangle^{1/2} = 0.03$. The density fields of the evolved models are presented in Figs 7 and 8. One can see that all large features obtained with both codes are very similar, while small-scale structures (important in the $n = +1$ runs) are slightly different. Also, the density field is smooth in CPPA while in AP^{3}M it is affected by the large scatter of the mass tracers in low-density regions.

4.3. Performance Comparison

Timing tests have been performed for both CPPA and AP^{3}M. The test runs were 60 steps on SUN 10/40 for 32^3 and 64^3 particles/cells, with low density contrasts (no mesh refinements in AP^{3}M). The results are given in Table 1. As we can see, CPPA performs one step 2–3 times faster. It has to be mentioned that in the non-linear regime in dense regions there are many fast moving particles in AP^{3}M, while in CPPA the velocity in a given cell is averaged over all mass contained in that cell, thus getting smaller. Hence, due to the CFL condition, a step in CPPA is larger than in Couchman's code, making CPPA still faster.

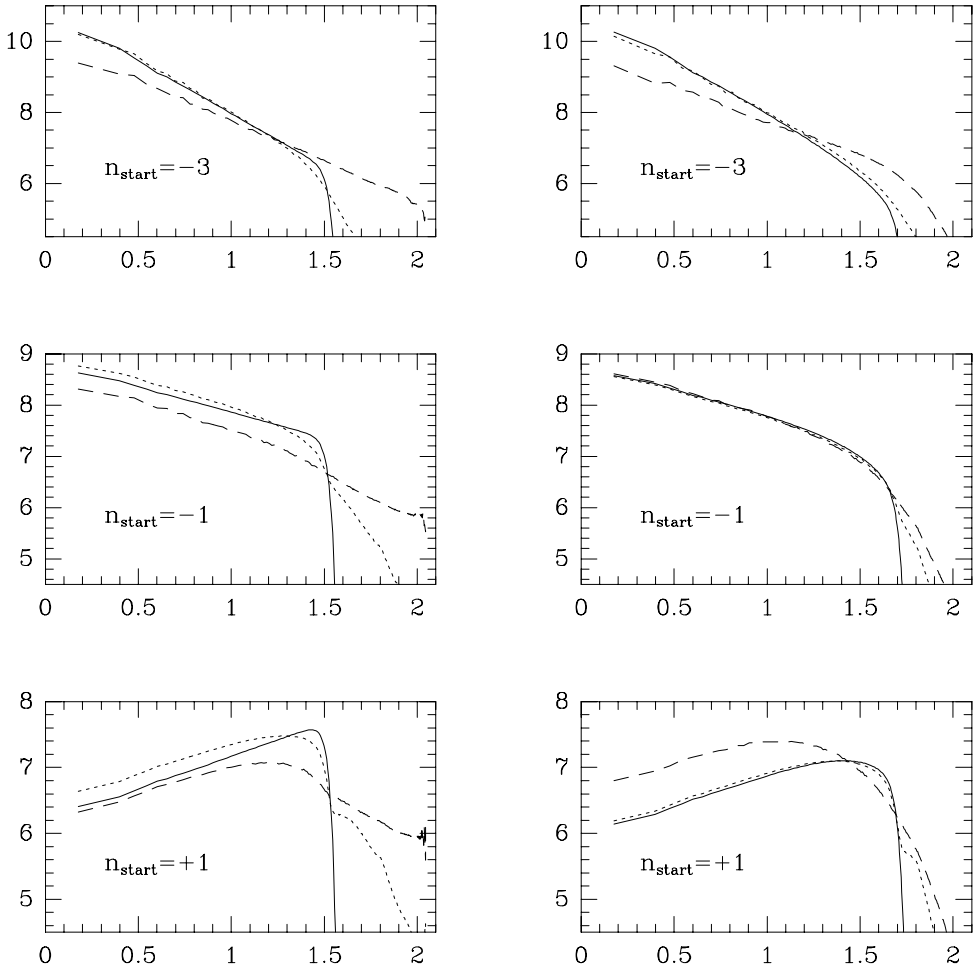

Fig. 4. Evolution of power spectra on 128^3 grid. **Horizontal axis:** $\log k$, **vertical axis:** $\log P(k)$. **Left:** CPPA, **right:** AP^{3}M. **Solid line:** initial conditions, **short dash:** weakly nonlinear stage ($\langle\delta^2\rangle^{1/2} = 0.3$), **long dash:** nonlinear stage ($\langle\delta^2\rangle^{1/2} = 2$).

5. Summary

CPPA has proven to be a fast and useful code that well reproduces the statistics of cosmic fields in large scales. In the examples presented here it lacks resolution on small scales, but presently it is running on large grids (up to 192^3) on SGI and CRAY machines. We are also working on improving its accuracy with AMR (Adaptive Mesh Refinement) techniques.

Acknowledgements. This work was supported by the KBN grant 2P-304-017-07. The simulations are partly performed on Cray computers at the Interdisciplinary

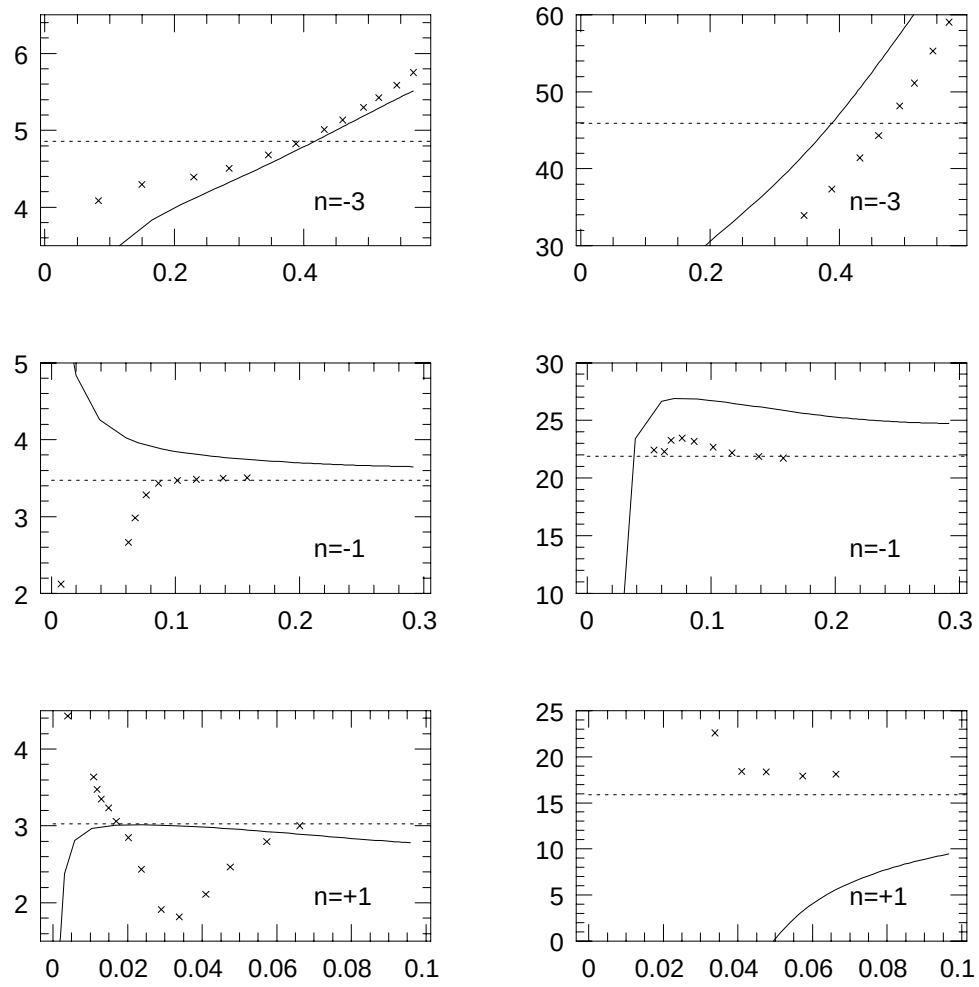

Fig. 5. Evolution of skewness (S_3) and kurtosis (S_4) of the density field versus density dispersion. 128^3 grid, Gaussian filter. **Horizontal axis:** $\langle\delta^2\rangle^{1/2}$ of smoothed density field, **vertical axis:** S_3 (**left**) and S_4 (**right**).
Solid line: PPA, **crosses:** AP^{3}M, **dashed:** perturbation theory.

Fig. 6. Cosmic density field for $\langle\delta^2\rangle^{\frac{1}{2}} = 2$. Simulation with CPPA code (left) and with AP^{3}M (right). Initial power indices: $n = -3$ (upper), $n = -1$ (middle), $n = +1$ (lower).

Center for Mathematical and Computational Modeling in Warsaw.

Fig. 7. Cosmic density field for $n = -3$ at $z = 2$. Simulation with AP^{3}M (left) and CPPA (right).

Fig. 8. Cosmic density field for $n = 1$ at $z = 2$. Simulation with AP^{3}M (left) and CPPA (right).

T a b l e 1

Execution times.

problem	execution time [s]			
	init	evol	total	per step
32^3 AP^{3}M	40	1129	1169	18.81
32^3 CPPA	29	371	399	6.18
64^3 AP^{3}M	261	8822	9083	147.04
64^3 CPPA	249	3987	4235	66.44

REFERENCES

Adams, J., Schwarztrauber, P., and Sweet, R. 1980, *FISHPAK, a Package of FORTRAN Subprograms for the Solution of Separable Elliptic Partial Differential Equations*, version 3.1, NCAR.

Catelan, P., and Moscardini, L. 1994, *Astrophys. J.*, **426**, 14.

Colella, P., and Woodward, P.R. 1984, *J. Comput. Phys.*, **54**, 174.

Couchman, H.M.P. 1991, *Astrophys. J. Letters*, **368**, L23.

Couchman, H.M.P. 1994, *preprint*, Cosmological Simulations Using Adaptive Particle-Mesh Methods, in http://www-hpcc.astro.washington.edu/simulations/DARK_MATTER/adapintro.html.

Gnedin, N.Y. 1995, *Astrophys. J. Suppl. Ser.*, **97**, 231.

Gunn, J.E., and Knapp, G.R. 1993, in *Sky Surveys*, B.T. Soifer, ed., ASP Conf. Series, 43, p. 267.

Juszkiewicz, R., Bouchet, F., and Colombi, S. 1993, *Astrophys. J. Letters*, **412**, L9.

Łokas, E.L., Juszkiewicz, R., Weinberg, D.H., and Bouchet, F.R. 1995, *MNRAS*, **274**, 730.

Peebles, P.J.E. 1980, *Large scale Structure of the Universe*, Princeton, Princeton University Press.

This figure "fig6.gif" is available in "gif" format from:

http://arXiv.org/ps/astro-ph/9609037v1

This figure "fig7.gif" is available in "gif" format from:

http://arXiv.org/ps/astro-ph/9609037v1

This figure "fig8.gif" is available in "gif" format from:

http://arXiv.org/ps/astro-ph/9609037v1